NASA TECHNICAL MEMORANDUM

NASA TM X-52153

MATERIAL AND GEOMETRY ASPECTS OF SPACE RADIATORS

by Seymour Lieblein and James H. Diedrich
Lewis Research Center
Cleveland, Ohio

TECHNICAL PAPER presented at Winter Meeting
of the American Nuclear Society
Washington, D. C., November 15-18, 1965

NATIONAL AERONAUTICS AND SPACE ADMINISTRATION · WASHINGTON, D.C. · 1965

MATERIAL AND GEOMETRY ASPECTS OF SPACE RADIATORS

by Seymour Lieblein and James H. Diedrich

Lewis Research Center
Cleveland, Ohio

TECHNICAL PAPER PRESENTED at
Winter Meeting of the American Nuclear Society
Washington, D. C., November 15-18, 1965

NATIONAL AERONAUTICS AND SPACE ADMINISTRATION

MATERIAL AND GEOMETRY ASPECTS OF SPACE RADIATORS

by Seymour Lieblein and James H. Diedrich

Lewis Research Center
National Aeronautics and Space Administration
Cleveland, Ohio

ABSTRACT

14772

Space-radiator materials and fin-tube geometry have a large influence on the ultimate size and weight of the radiator. Many factors, in turn, influence the requirements for materials and geometry, such as meteoroid damage protection, structural integrity, vehicle integration, and fluid compatibility. Similarly, there is a wide variety of materials and geometries that can be considered. It appears that a completely satisfactory solution of the materials-geometry question for advanced Rankine power systems is not yet in hand.

INTRODUCTION

Designers of advanced nuclear space power systems are very much concerned with the size and weight of the radiators required to dissipate the waste-heat loads. The radiator size and weight are each governed by several principal factors or variables. The size of the radiator is determined by the design heat load and the external radiation heat-transfer rate. External radiation heat transfer is a function primarily of the temperature of the working fluid, the emittance of the radiator surface, the specific radiator geometry and material, and the internal fluid flow. The temperature of the radiator working fluid is determined by the cycle optimization and design, which has been the subject of many system studies. The surface emittance, for many radiator materials, will depend on the applied coating. Recent tests of high temperature coatings in vacuum conducted under contract by the Pratt & Whitney Company (ref. 1) have shown that stable coating operation up to 10,000 hours can be achieved at emittance levels up to 0.9 (fig. 1). Similarly, it appears that the internal flow associated with condensing potassium for radiator applications is also well in hand (e.g., refs. 2 to 4). Thus, the remaining variable governing the magnitude of the radiator area is the specific radiator geometry and material.

The weight of a radiator is determined directly by the radiator materials and structure, which include both the basic heat transfer components (fin and tube, headers) and the structural support and vehicle-interface components. Material selection is based on considerations of internal fluid compatibility (cycle temperatures and alkali metal used), meteoroid damage protection, structural loads,and simplicity of fabrication and construction. Unfortunately, many of these requirements are frequently

in conflict. Radiator geometry can also be utilized to enhance external heat transfer, meteoroid protection, and structural support. Many configurations are possible, and there is a strong interrelation between geometry and materials considerations.

This report will examine some aspects of the material-geometry coupling with respect to such factors as meteoroid protection, fin-tube configuration,and panel segmentation, as obtained from recent studies conducted by the NASA-Lewis Research Center.

METEOROID PROTECTION

Meteoroid Flux

Considerable work has been done recently at the Lewis Research Center on defining the meteoroid hazard as it exists in space. As a result of analysis of particle-flux data obtained from the various satellite experiments, from photographic and radar meteor observations, and studies of the zodiacal light, it appears that a good part of the observed data variations and discrepancies can be explained on the basis of the existence of two distinct types of dust particles. One class of particles is known to be in orbit around the sun (heliocentric orbit). These particles constitute the cometary meteoritic particles that are detected by radar and photographic observations (ref. 5) and the zodiacal space dust. The second type of particle is believed to be in orbit around the earth (geocentric orbit). It is further believed that the earth-orbiting meteoroids are the particles that most of the satellite experiments are detecting. An early discussion of this concept is given in reference 6. On the basis of a more recent analysis by I. J. Loeffler[1], analytical distributions for the meteoroid flux versus particle mass have been established as shown in figure 2. The figure shows the deduced curve for the heliocentric flux and for the geocentric flux at three altitudes above the surface of the earth. In general, the geocentric flux will decrease with increasing altitudes.

For the geocentric flux, the hypothesis considers that these particles are most likely in direct orbit around the earth. Depending on the relative orbits of particle and spacecraft, the relative impact velocity would be in the order of 0 to 11 km/sec with probable values approximated by the circular orbital velocity (e.g. 7.35 km/sec at 1000 km altitude). It is also believed that the typical density of these particles is of the order of 1 gm/cm^3. For the heliocentric-cometary meteoroids the work of the Harvard Astronomical Observatory has indicated that the average density of such particles is on the order of 0.2 gm/cm^3 in the photographic range (ref. 7), and 0.5 gm/cm^3 in the radar range. Estimates of a representative velocity

[1]Individuals named in the text, unless otherwise indicated, are members of the Flow Analysis Branch of the Lewis Research Center.

for the heliocentric meteoroids have also been recently made. Detailed information concerning the characteristics of the cometary meteoroids have been obtained chiefly from photographic observations. However, there is a lower threshold of both particle mass and velocity that can be photographed. Consequently, there are more meteoroid particles of lower velocities than have been observed. In a detailed analysis of a large number of meteor photographic plates conducted by C. D. Miller, a revised velocity distribution has been determined for sporodic cometary meteors based on a correction of the minimum photographability of meteor trails. A log-normal actual velocity distribution was obtained and integrated with respect to an impact-damage relation based on the 2/3 power of impact velocity to yield an effective velocity for the heliocentric distribution from 17 to 20 km/sec.

As a result of these analyses, average meteoroid impact velocities for both the geocentric and heliocentric distributions have been reduced considerably compared with the previous values of around 30 km/sec. This means that not only has the magnitude of the hazard itself been reduced, but also that the applicability of laboratory impact data is more significant. The light-gas gun is currently firing routinely at 7.6 km/sec, and it appears that velocities up to 10 km/sec may be obtained with this device. Thus, the degree of extrapolation required can be considerably reduced, and more confidence can be placed on the suitability of impact results obtained in laboratory hypervelocity facilities.

Recent results obtained from the Pegasus II and III meteoroid detection satellites are also shown in figure 2. The two open symbols represent the calculated points for the 8- and 16-mil (0.2- and 0.4-mm) thickness sensors. These points were calculated according to the conditions for the geocentric flux hypothesis (ρ = 1 gm/cm^3 and V = 7.35 km/sec). The calculation of the 16-mil data point based on heliocentric flux is shown by the solid symbol (based on ρ = 0.5 gm/cm^3 and V = 20 km/sec). It is seen that good agreement is obtained between these preliminary data and the analytical model for the flux. It should be pointed out here that the region of interest for advanced system radiator designs in figure 3 extends from particle mass level of about 5×10^{-4} gm and up. This range is represented roughly at the lower limit by the Pegasus data and in the upper range by the photographic meteor data. It is felt, therefore, that the model of figure 2 is a fairly representative description of the meteoroid flux in this region of interest.

Another aspect of this recent work, namely, the very low density of the heliocentric particles, has indicated that we cannot consider meteoroids as solid homogeneous particles. It is apparent that these particles, because of their constituents and low bulk density, must be of a "fluff-ball" nature with some distribution of mass. In order to determine whether there is a difference in the impact characteristics of "fluffy" particles and solid particles of the same mass, Dr. T. D. Riney of the General Electric Company has been contracted by the Lewis Research Center to conduct theoretical studies of the impact characteristics of particles of heterogeneous mass distributions and low bulk densities.

Hypervelocity Impact Results

Considerable contract work has been done in the past year by the General Motors Corporation in Santa Barbara on hypervelocity impact into various simulated radiator targets and materials using a light-gas gun (ref. 8). As indicated previously, projectile velocities of 7.6 km/sec can be achieved with the light-gas gun for routine firing of spherical projectiles in the diameter range of 1/16 to 1/8 in. (1.6 to 3.2 mm). The relation between projectile size for several common projectiles and radiator design meteoroid hazard parameter $\frac{A_V \tau}{-\ln P(o)}$ (ref. 9) is shown in figure 3(a) for an energy level equal to the comparble representative meteoroid particle in space. The corresponding variation of meteoroid particle minimum mass at 20 km/sec against which the radiator must be protected is shown in figure 3(b). Typical radiator designs for power systems in the 300- to 1,000-kilowatt class with lifetimes τ of 365 to 500 days, no-damage probabilities $P(o)$ of 0.90 to 0.98, have values of the hazard parameter from around 10^6 to 5×10^7 ft^2-days (0.9×10^5 to 4.7×10^6 m^2-days). For this range of the hazard parameter, it is seen from figure 3 that the light-gas gun produces projectile energies comparable to those of the applicable meteoroid particles in space.

Damage modes.- Initial results of the hypervelocity impact tests are given in references 10, 11, and 12. These results indicated that radiator tubes can sustain several modes of critical damage (fig. 4). In addition to cratering of a surface and actual perforation of a tube wall, dimpling and spalling of the inner surface of the tube can be obtained at thicknesses larger than that required to prevent perforation. Dimpling of the inner surface may be undesirable since it causes a restriction of the flow passage. For spall, the release of metal fragments or particles into the radiator circulating fluid in a zero-gravity environment is not considered desirable when rotating components are present in the flow circuit. Perforation, of course, will result in a loss of the working fluid.

The crater, perforation, dimple, and spall characteristics of a wide range of materials have been determined in the General Motors program. Some of the results, as calculated by N. Clough, are listed in table I.

TABLE I. - RESULTS OF HYPERVELOCITY IMPACT TESTS

Material	[a]Cratering coefficients, γ	[b]Rear-surface damage factors		
		Dimple t/P_∞	Spall t/P_∞	Perforation t/P_∞
2024-T6 aluminum	1.97	2.5	2.3	1.7
316-Stainless steel	1.67	2.4	1.9	1.4
Columbium-1 percent Zr	1.39	4.5	4.0	1.7
Beryllium	2.05	---	---	---
Graphite (ATJ)	1.18	---	---	---
Inconel-718	1.55	3.0	2.5	---
L-605	1.77	2.5	2.1	1.7
A-286	1.99	2.4	1.9	1.4
Vanadium	1.38	---	---	---
Molybdenum	1.57	---	---	---

[a]Room temperature values. Additional data in reference 12.
[b]Threshold or incipient values.

The cratering coefficient γ in table I refers to the empirical correlation factor used in the relation for estimating the crater depth in a thick target P_∞, as indicated by the following equation.

$$\frac{P_\infty}{d} = \gamma\left(\frac{\rho_p}{\rho_t}\right)^{1/2}\left(\frac{V}{\sqrt{gE_t/\rho_t}}\right)^{2/3} \qquad (1)$$

where d is the particle diameter, ρ_p is the particle density, V is the impact velocity, ρ_t is the target density, E_t is the target modulus of elasticity, and g is the gravitational constant. Normally, if the correct property parameters are used, the value of γ should not vary much among different materials. In the past a uniform value of 2.0 has been used in radiator-armor calculations (e.g., refs. 9 and 13). As can be seen in table I, the cratering coefficient varied considerably for the materials tested. This means that we really do not completely understand the impact phenomena and do not know the proper material property or strength parameters and correlating functions that will unify the data. Table I further indicates that specific impact tests should be conducted for any particular material that is finally used in an actual radiator design.

It is also interesting to note that graphite shows a very low cratering coefficient, indicating that very shallow craters are produced in this material. This may suggest that graphite would be a good armor material, and that further investigations of the impact characteristics of conventional graphite and pyrolytic graphite are in order.

In a similar fashion, wide variations were obtained in the dimple, spall, and perforation damage factors. These factors defined in figure 4 are listed in table I as the ratio of the thickness corresponding to the onset of the particular damage mode to the crater depth in a semi-infinite thick target P_∞ as given by equation (1). In particular, it is noted that columbium - 1-percent zirconium requires a very large thickness to prevent spall. Such a large thickness factor would render this material too heavy in anticipated radiator use. However, this would not necessarily be the case if the design does not require the complete elimination of spalling. In this respect, it should be noted that the use of an electromagnetic or other type of nonrotating pump in a circulating loop of an all-liquid segmented radiator would make the design to defeat spalling unnecessary. Since there are no moving parts in the electromagnetic pump circuit, the possibility of catastrophic damage from the release of spalled particles would not be present in this type of system. The indicated reduction in weight because of thinner allowable tube walls in this case might easily compensate for the added weight and reduced efficiency of the pump.

The wide variation of critical damage factors obtained for the damage modes and materials covered in table I has been reflected in an equally wide variation of radiator specific weights. Comparative weight calculations for a central fin-tube radiator based on these new damage factors are given in reference 12. In those plots, it was shown that a substantial weight reduction can be obtained with single-material tubes (no inner liner), if the avoidance of perforation rather than spall can be adopted as the design criterion. However, the bimetallic configurations with inner liners and beryllium or graphite armor continued to evince the least weights. A comparison of such lined tubes with stainless-steel and columbium-alloy tubes designed for the avoidance of perforation is given in figure 5. Specific weights were computed according to the method of reference 14 using the meteoroid flux, velocity, and density values proposed in reference 5 for 300 kilowatts power output, 10,000 hours, and $P(o) = 0.96$.

The graphite armored tubes in figure 5 were computed for three values of bulk density: one corresponding to a normal ATJ graphite; one for a full-density pyrolytic graphite; and the other for a low-density expanded pyrolytic graphite composite construction (e.g., ref. 15). The value γ used for the calculation of armor thickness for the expanded pyrolytic graphite was determined from the experimental penetration depth data of reference 15 and an assumed value of full-density modulus of elasticity (eq. (1)). In the absence of specific experimental data, the tube-liner dimple factor (a_d) in the equation for armor thickness for the expanded graphite was taken as 1.75. This value of damage factor with lined beryllium tubes corresponds to a ratio of liner dimple height to inner diameter of around 0.25. The single curve shown in figure 5 for the expanded pyrolytic-graphite armor represents the mean of a band of values

($\pm$ 0.25 lb/kw or $\pm$ 0.11 kg/kw) obtained from variations in the estimated values of liner damage factor (1.6 to 1.75) and thermal conductivity (30- to 80-percent full-density value).

Effect of liquid fill.- All impact work to date has been done with plates and empty tubes. The question therefore arises: what will be the effect of the presence of a fluid inside the tube and, in particular, the effect of a liquid such as the liquid metals? In an attempt to answer this question, impacts were conducted into tubes filled with water, and in general it was found that there is very little effect because of the presence of the internal liquid. Typical results are shown in figure 6. The figure shows the result of identical impacts into an empty and water-filled tube composed of a stainless-steel liner and surrounding cast-aluminum armor. The fairly sizable dimple obtained in the empty tube is noticeably suppressed when water is present in the tube. The same result was observed for tubes of smaller diameters. Comparable tests were conducted on stainless-steel tubes to determine the effect of liquid fill on spalling, and here too, similar results were observed. It appears therefore that results of tests with empty tubes, since they tend to be conservative, can be used for radiator-design applications. Tests are now being set up at General Motors to determine the comparative impact into a tube filled with NaK and heated to 1300° F.

Beryllium impact.- The effect of hypervelocity impact on beryllium-armored tubes has also been investigated. Preliminary results are reported in reference 16. In general, it has been found that beryllium will crack on impact by hypervelocity particles. Some results of this cracking phenomenon are shown in figure 7. The target on the left represents the best result obtained from several materials and fabrication processes that are currently available for fabricating a beryllium-armored tube. A large spalled area is observed around the point of impact, and cracks were seen to eminate radially from the crater area. In some cases, circumferential and longitudinal cracks were also observed. Attempts were made to reduce the cracking by placing internal reinforcements within the beryllium. The first reinforced tube contained fine-kinked stainless-steel fibers randomly dispersed in the beryllium. For the second reinforced tube, two cylinders of stainless-steel wire mesh were inserted concentrically within the beryllium at two radial positions. Impact into both of these reinforced targets showed only little reduction in the observed cracking phenomenon as indicated in figure 7 by the two central tubes.

Another aspect of the beryllium cracking was the thought that in the event of multiple impacts (i.e., if a second impact occurred adjacent to an earlier impact) large sections of the cracked beryllium armor might be removed. A double impact was therefore obtained by firing into a beryllium tube with equal-energy impacts approximately 180° apart. As shown by the target on the right of figure 7, no separation or removal of armor was observed. However, a crack joining the two crater areas did appear.

Sections of these targets have also been taken to obtain a better picture of the damage within the beryllium armor as shown in figure 8. The nonreinforced tube showed considerable cracking within the beryllium armor in the area near the crater and also in the region opposite the location of impact. A delamination of the beryllium-to-liner bond was also observed in this particular case. The cross-section macrophotographs of the wire-mesh reinforced tubes are also shown in figure 8. Here, too, the internal cracking was clearly evident, and the reinforcements reduced the cracking only slightly.

The beryllium cracking in itself may not be critical in a radiator design because the tube armor is not generally designed to transmit structural loads. Furthermore, any effects of delamination or cracking on the heat transfer through the tube would be limited to the local area around the tube and, in general, would not constitute a large percentage of the total radiator area. However, the long-term aging, cycling, or vibration effects on a cracked beryllium section are not known at this time.

Impacts into several conventional grades of graphite have also been conducted and a similar, though perhaps less severe, cracking tendency has been observed (ref. 16). There is evidence, however, that expanded pyrolytic graphite structures of less than full theoretical density may have acceptable impact characteristics (ref. 15). Further consideration of graphite may therefore be warranted, although serious inherent problems with respect to brittleness, low strength, and bimetallic bonding are recognizable (somewhat similar to the situation with beryllium).

FIN-TUBE GEOMETRY

Configurations

There are a wide variety of fin-tube shapes and geometries that can be used in a radiator design. These configurations can involve either an outer-armor section bonded on an internal liner of dissimilar materials, or they can be composed of monometallic unlined tubes. Some of the configurations that have been under analysis are shown in figures 9 and 10. The geometries of figure 9 represent solid-conducting fin geometries. In these configurations, heat is transferred along the fin by conduction and is then ultimately transferred into space by radiation. The upper left section represents the conventional central fin tube geometry armor sleeve bonded to an internal high-strength liner. For cylindrical-radiator configurations, the block open fin geometry can be used in one of two forms: in one, the armor block completely surrounds the tube; in the other, as indicated by the dashed lines, the armor block is bonded only to the upper portion of the tube liner. A block double fin geometry can also be used, as indicated in

the lower configuration on the left, in which an armor block is between a sandwich of fins and an internal liner is bonded to the armor block.

The bumper principle can also be used, as indicated by the configurations on the right in figure 9. In these geometries, the tube is connected to the fin by means of a thin strut. Protection in this form is achieved by the action of the fin as a bumper in breaking up the impacting particle and spreading the energy of impact over a greater area of the tube. A double bumper fin configuration can also be obtained by the use of an identical fin on the lower surface as shown in the lower right of figure 9. It should be noted that the tubes in the bumper-fin geometries are monometallic (without internal liners).

In some cases, it may be desirable to use fins with thermal conductivities higher than those available from conventional high-strength metals. Such a high conductivity fin can be obtained for the temperature levels of the advanced systems by a clad fin in which two thin wafers of stainless steel or possibly a high-strength titanium alloy cover an inner core of copper. Stainless steel-copper clad sheet has been widely used in heat exchanger and other industrial applications. For ease of fabrication, the clad material should generally be the same as the tube material.

The two configurations in figure 10 present geometries utilizing the vapor chamber fin principle. These configurations are essentially double fin geometries in which an internal capillary medium such as a wick or a fibrous material lines the inner walls of the chamber formed by the fins connecting two adjacent tubes. The capillary material is charged with a transport fluid which is boiled off the tube surface and condenses on the fin surface, thus generating a fin of essentially constant temperature. The boiling surface is continuously supplied with working fluid through the capillary medium. The constant temperature aspect of the fin results in a very high radiating effectiveness and a reduced area for the entire radiator. The vapor-chamber-fin concept can be used in either the block or bumper forms as shown in figure 10 or in other possible configurations and geometries. In an actual radiator construction, it will be necessary to segment the vapor-chamber fins longitudinally, so that a meteoroid puncture would not release the transport fluid from the entire tube length. For single-phase-flow (noncondensing) radiators involving axial variations in temperature, it may be desirable to use individual fin chambers that are relatively short in length and separated longitudinally. Such a construction may be necessary to reduce the effects of axial temperature gradients in the tube on the fin-chamber internal flow, and it may also be helpful structurally.

There is another class of radiator tube geometries for cylindrical-vehicle configurations involving involute reflectors instead of or in conjunction with conducting fins (refs. 4 and 17). However, these geometries are not considered in this survey. In any event, it is important to point out here that the particular tube geometry selected

for a radiator design will exert a large influence on the radiator vulnerable area (and therefore armor requirement) and total area and, consequently, total weight.

Comparisons

In general, calculations have shown that bumper- or block-vapor-fin radiators will give reductions in radiator planform area of around 20 percent and reductions in weight ranging from 30 to 50 percent compared with the solid conducting fin configurations shown in figure 9. An illustration of the effectiveness of the bumper-vapor fin in achieving low specific weight is shown in figure 11. This figure compares calculated radiator specific weights as a function of the ratio of the tube wall thickness δ_t with the required armor thickness δ_a for both the block- and bumper-vapor fin geometries constructed of stainless steel. Recent preliminary tests at General Motors, shown by the sketch and vertical line in figure 11, have indicated that, as a result of the bumper action, fairly small wall thicknesses can be achieved without tube inner-surface spalling. The fin thickness for the calculations of figure 11 was determined on the basis of a 0.90 probability that 75 percent of the fin chamber segments would remain unpunctured.

The calculations also show that the use of the vapor-chamber-fin concept can permit the design of radiators with fewer, larger diameter tubes with considerably wider spacings between tubes compared with conducting-fin radiators without large penalties in weight. Such radiator configurations may be desirable for considerations of fabrication, assembly, structural support, and vehicle integration.

With respect to vapor-fin-chamber operation, it should be noted that it is desirable to have fins of high thermal conductivity so that in the event a fin chamber is punctured the fins can act in the normal conducting manner and still maintain a fair level of radiating effectiveness. In this way a large number of punctured segments can be tolerated in the design (to reduce fin thickness) without incurring a large degradation in radiating effectiveness. Such a high conductivity fin can generally be obtained with a clad copper fin as described earlier. However, the advantages of high conductivity fin materials will be essentially negated for configurations with longitudinally separated fin chambers, as may be indicated for single-phase-flow (noncondensing) radiators.

A large number of fin-tube geometries and materials have been analyzed with respect to total radiator weight and area by R. P. Krebs, H. C. Haller, B. T. Lindow, and A. V. Saule, in references 14, 18, 19, and 20. Some of the problems involved in developing the materials and configurations indicated in each case have also been assessed. The results of these comparisons are summarized in table II. Presented in the table are several general classes of radiator configurations, the estimated range of specific weights obtainable for a 500-kilowatt output

Rankine cycle, and the anticipated problem areas associated with the development of the particular fin-tube geometry. The specific weights presented were calculated for a direct-condensing radiator including headers but with no allowance for support structure. A comparable relative picture would be obtained for all-liquid flow radiators. The survival probability of 0.92 corresponds to an overall value of 0.98 for an eight-segmented radiator.

TABLE II. - COMPARISON OF RADIATOR SYSTEMS
500 kW(e), 10,000 HOURS, P(0) = 0.92, 1700° R

Class	Specific weight, lb/kW(e)	Problem
Beryllium bumper-vapor fin (with tube liner)	1.0 to 1.2	1. Cracking 2. Coatings 3. Bond 4. Capillary flow 5. Capillary corrosion 6. Chamber fabrication
Beryllium armor and fins (solid conducting, with tube liner)	1.7 to 2.1	1. Impact cracking 2. Emittance coatings 3. Bimetallic bonding
Graphite armor and fins (solid conducting, with tube liner)	2.0 to 3.0	1. Bimetallic bonding 2. Low strength
Titanium or stainless-steel clad bumper-vapor fin	1.9 to 2.6	1. Capillary internal flow 2. Fin-chamber fabrication 3. Clad conductivity and bond
Titanium or stainless-steel clad bumper-conducting fin	2.7 to 3.6	Clad conductivity and bond
Solid titanium or stainless-steel bumper-conducting fin	3.6 to 4.6	None

In general, as would be expected, the lighter the weight the greater the number of problems involved. On the basis of table II and earlier discussions, it is evident that considerable effort would be required to satisfactorily develop beryllium for use in space radiators. The reduction of impact cracking and brittleness, the development of liner-armor bonding techniques and stable high emittance coatings, and high cost are recognized as the principal development problems with beryllium. Similar difficulties are apparent with the graphites. The need for surface coatings may be eliminated in this case because of the naturally high emittance of graphite, but this is probably counterbalanced by the relatively low strength of the material.

For the clad fin geometries in table II, the low values of the weight range correspond to the titanium clad. There is sufficient incentive then to investigate corrosion-resistant titanium alloys with acceptable strength levels and meteoroid-impact resistance at radiator temperatures.

In general, the use of conventional materials with clad fins and no inner liner can produce reasonable weights and easily fabricated structures with few anticipated problems. However, the endurance and stability of the cladding with respect to bond and thermal conductivity will have to be verified. For the vapor-chamber concept, trouble may be experienced in the fabrication, sealing, and buckling resistance of the fin chambers. Furthermore, the vapor and liquid flow within the fin chamber is a relatively little known factor which will require considerable study.

RADIATOR SEGMENTING

In any event, for all fin tube configurations, it is desirable to use segmented radiators in order to achieve redundancy in the case of high power systems and manned missions. The most direct way of achieving radiator redundancy is to use liquid radiators in parallel with a convectively cooled condenser. In this manner, each radiator loop is completely independent of the others, and a meteoroid puncture will result in the loss of only the cooling capacity of that particular radiator circuit. Another concept that can be used to obtain radiator redundancy is the shared-fin principle. In this concept, instead of individually separated radiators the tubes of a given radiator are connected alternately to different headers. Thus, there are several independent tube circuits within a radiator panel. The advantage of this type of configuration is that, if a tube is punctured and coolant is lost from its circuit, the tube and its fin can still receive heat from the adjacent tubes and fins on either side. Thus, the radiation from the surfaces of the punctured fin and tube is not reduced to zero, and a smaller reduction in radiating effectiveness will result for the entire radiator system.

These redundancy concepts are illustrated in figure 12. On the lower right part of the figure is the conventional segmented-radiator concept in which each radiator is attached to a part of the condenser. In the upper left of the figure is the shared-fin concept in which each tube is connected to a different header to form the independent circuits.

Calculations have been made by M. Colaluca to determine the radiating effectiveness of a shared-fin radiator when one of the tube circuits is punctured. The results are shown in the figure. The dashed curve represents the variation in radiating effectiveness with the number of independent circuits for the separated radiator configuration shown on the right. The solid curve represents results for a comparable shared-fin radiator as a function of the number of circuits. In general, depending on the specific fin-tube geometry and materials used, the

radiating effectiveness for the shared-fin concept with one circuit punctured would be from 5 to 10 percent greater than that of the separated radiator configuration for three to six circuits. With a vapor-chamber-fin geometry and a shared-fin or segmented-overall configuration, the radiator will progressively degrade in thermal effectiveness as meteoroid punctures are incurred in time. Thus, the space vehicle will be faced with a power loss problem. If the power loss becomes too severe, in the case of a manned vehicle, there still exists the possibility of manual repair of the punctured radiator circuit. After the holes in the defunct circuit are welded, the repaired radiator circuit can then be reactivated and the power increment restored. With this concept, the principal development problems are expected to be associated with the vapor-chamber-fin construction and operation.

The use of segmented radiators requires that several liquid radiators and circulating pumps be utilized in conjunction with a convectively cooled condenser. This implies an additional weight penalty and power drain because of the additional circulating pumps and their drives. It would be desirable, therefore, to still maintain a redundancy concept for the radiator, which would not involve the need for circulating pumps. A possible scheme that does this is the use of vapor-chamber fins to cool the vapor condenser directly. One form of such a configuration is shown schematically in figure 13. In this figure, the condenser is in the form of an annulus with the fluid flowing in the longitudinal segments of the annular passages. The outer surface of the condenser is covered in a spline fashion by tapered vapor-chamber fins. These fins are segmented along the length in order to reduce the degradation effect of the impact of an individual chamber. In this configuration, the ordinary capillary vapor-chamber fin operation is indicated by the sketch on the right of the figure. Armor protection is eliminated on the condenser because of the complete coverage of the condenser outer surface by the tapered vapor fins. For this arrangement, the net radiation is approximately that of the circumscribed cylinder so that, in general, it will not be more compact and will consume more internal volume than a corresponding cylindrical radiator. However, if feasible it can eliminate the need for the circulating pumps.

CONCLUDING REMARKS

On the basis of the radiator studies discussed herein, it appears that there is no one best configuration or recommended approach to the radiator problem for high-power-level systems. In general, the lower the specific weight the greater the development problems and vice versa. Selection appears to be primarily a matter of system requirements and associated trade-offs. A path of least resistance can be obtained with the use of conventional materials and bumper geometries, although at the expense of additional weight. However, if the designer is more adventurous, he might consider using vapor fins. In this case, a basic radiator

configuration could consist of a monometallic vapor-chamber fin geometry utilizing the bumper-protection principle with either stainless-steel or titanium-alloy tubes and fins. As indicated previously, a copper-core clad fin is desirable to reduce the degradation of radiating effectiveness when individual vapor chamber fins are punctured. It is also believed that some form of shared fin or segmenting will be necessary with a liquid-flow radiator in order to reduce the possible catastrophic results of an unexpected meteoroid penetration.

REFERENCES

1. Emanuelson, R. C.: Determination of the Emissivity of Materials. NASA CR-54444, 1965.

2. Sawochka, S. C.: Thermal and Fluid Dynamic Performance of Potassium During Condensing Inside a Tube. Paper Presented at AIAA Rankine Cycle Space Power System Specialist Conf., NASA Lewis Research Center and TRW, Inc., Cleveland (Ohio), Oct. 26-28, 1965.

3. Gutierrez, O. A.; Sekas, N. J.; Acker, L. W.; and Fenn, D. B.: Potassium Condensing Tests of Horizontal Convective and Radiative Multitube Condensers Operating at 1250° F to 1500° F. Paper Presented at AIAA Rankine Cycle Space Power System Specialist Conf., NASA Lewis Research Center and TRW, Inc., Cleveland (Ohio), Oct. 26-28, 1965. Also available as NASA TMX-52148, 1965.

4. Fraas, A. P.: Design and Development Tests of Direct-Condensing Potassium Radiators. Paper Presented at AIAA Rankine Cycle Space Power System Specialist Conf., NASA Lewis Research Center and TRW, Inc., Cleveland (Ohio), Oct. 26-28, 1965.

5. Clough, Nestor; and Lieblein, Seymour: Significance of Photographic Meteor Data in the Design of Meteoroid Protection for Large Space Vehicles. NASA TN D-2958, 1965.

6. Loeffler, J.; Clough, N.; and Lieblein, S.: Recent Developments in Meteoroid Protection for Space Power Systems. Paper Presented at Third Biennial Aerospace Power Systems Conf., AIAA, SAE, ASME, Interagency Advanced Power Group, and IEEE, Phila. (Pa.), Sept. 1-4, 1964.

7. Verniani, F.: On the Density of Meteoroids. II. - The Density of Faint Photographic Meteors. Il Nuovo Cimento, Series X, Vol. XXXIII, N. 4, pp. 1173-1184.

8. Anon.: Research Facilities of the Aerospace Operations Department. Rept. No. ER 62-201A, Defense Research Labs., General Motors Corp., 1962.

9. Loeffler, I. J.; Lieblein, Seymour; and Clough, Nestor: Meteoroid Protection for Space Radiators. Power Systems for Space Flight, Morris A. Zipkin and Russell N. Edwards, eds. Vol. 11 of Progress in Astronautics and Aeronautics, Martin Summerfield, ed., Academic Press, 1963, pp. 551-579.

10. Lieblein, Seymour; Clough, Nestor; and McMillan, A. R.: Hypervelocity Impact Damage Characteristics in Armored Space Radiator Tubes. NASA TN D-2472, 1964.

11. Diedrich, James H.; and Stepka, Francis S.: Investigation of Damage to Brittle Materials by Impact With High-Velocity Prejectiles into Glass and Lucite. NASA TN D-2720, 1965.

12. Clough, Nestor; and Diedrich, James H.: Results of Hypervelocity Impact Into Radiator Materials. Paper Presented at AIAA Rankine Cycle Space Power System Specialist Conf., NASA Lewis Research Center and TRW, Inc., Cleveland (Ohio), Oct. 26-28, 1965. Also available as NASA TMX-52142, 1965.

13. Diedrich, James H.; and Lieblein, Seymour: Materials Problems Associated With the Design of Radiators for Space Powerplants. Power Systems for Space Flight, Morris A. Zipkin and Russell N. Edwards, eds. Vol. 11 of Progress in Astronautics and Aeronautics, Martin Summerfield, ed., Academic Press, 1963, pp. 627-653.

14. Krebs, Richard P.; Haller, Henry C.; and Auer, Bruce M.: Analysis and Design Procedures for a Flat, Direct-Condensing, Central Finned-Tube Radiator. NASA TN D-2474, 1964.

15. Holl, Richard J.; and Goldstein, A.: Application of Pyrolytic Graphite to Space Radiators. Preprint 65-288, American Institute of Aeronautics and Astronautics, July 1965.

16. Diedrich, James H.; Loeffler, Irvin J.; and McMillan, A. R.: Hypervelocity Impact Damage Characteristics in Beryllium and Graphite Plates and Tubes. NASA TN D-3018, 1965.

17. Hwang-Bo, H.: Optimization of Some Radiators with Fins and Evolute Reflectors. Paper No. 65-WA/HT-17, ASME, 1965.

18. Haller, Henry C.: Analysis of a Double Fin-Tube Flat Condenser-Radiator and Comparison With a Central Fin-Tube Radiator. NASA TN D-2558, 1964.

19. Haller, Henry C.; Lieblein, Seymour; and Lindow, Bruce G.: Analysis and Evaluation of a Vapor-Chamber Fin-Tube Radiator for High-Power Rankine Cycles. NASA TN D-2836, 1965.

20. Haller, Henry C.; Lindow, Bruce G.; and Auer, Bruce M.: Analysis of Low-Temperature Direct-Condensing Vapor-Chamber Fin and Conducting Fin Radiators. NASA TN D-3103 (July 1965).

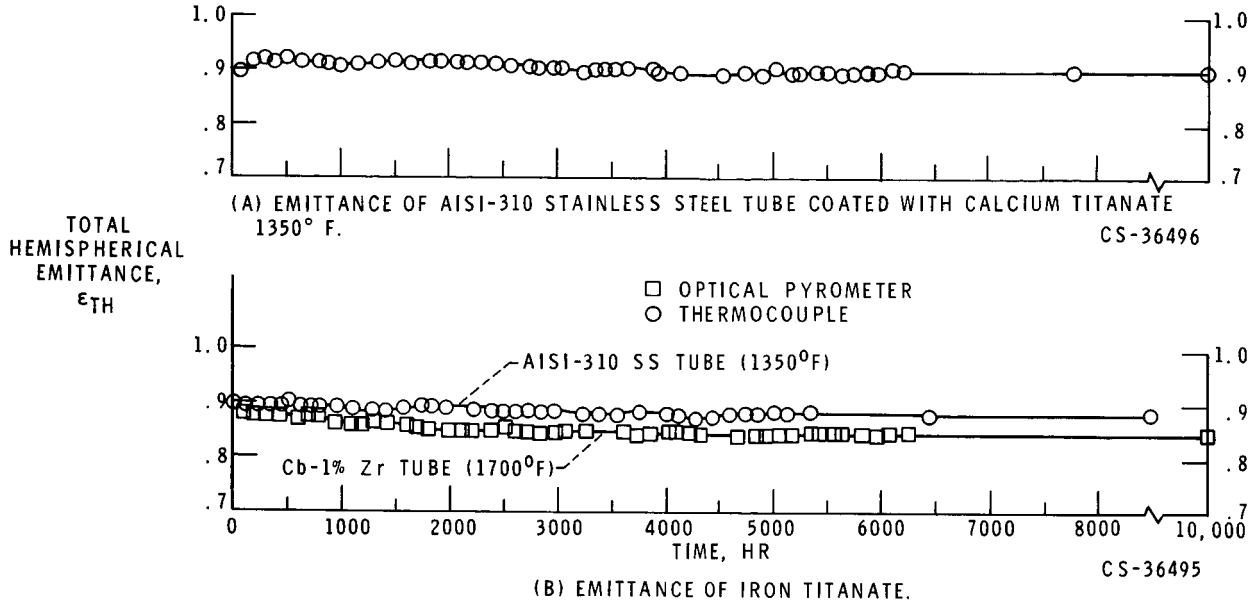

FIG. 1. - LONG-TERM ENDURANCE OF HIGH-TEMPERATURE SURFACE COATINGS.

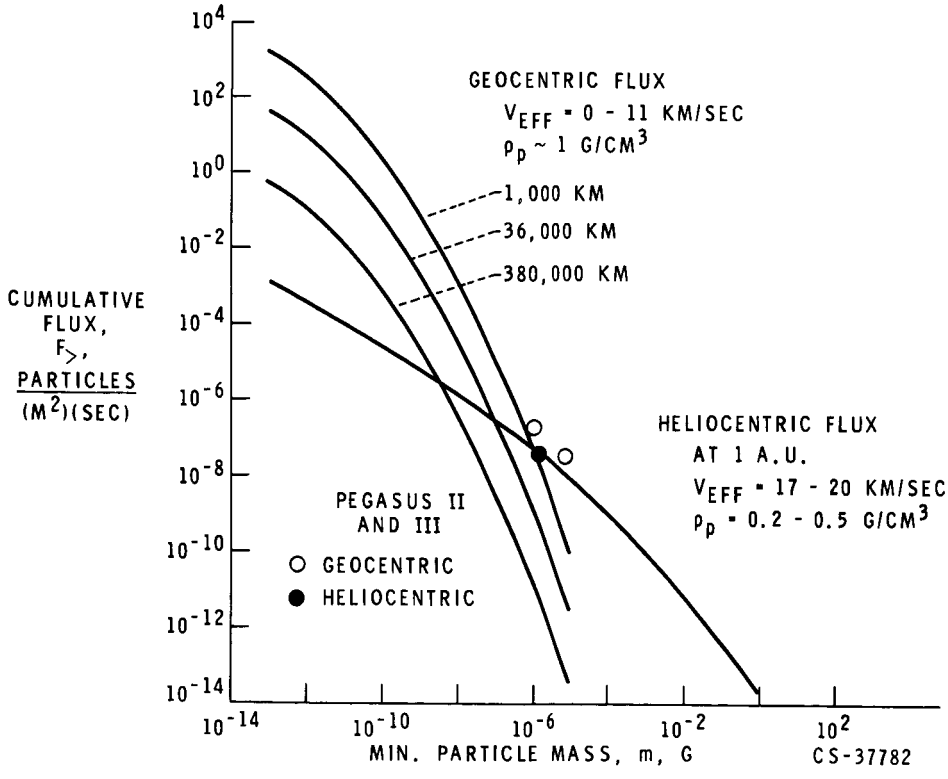

FIG. 2. - METEOROID FLUX-MASS VARIATION.

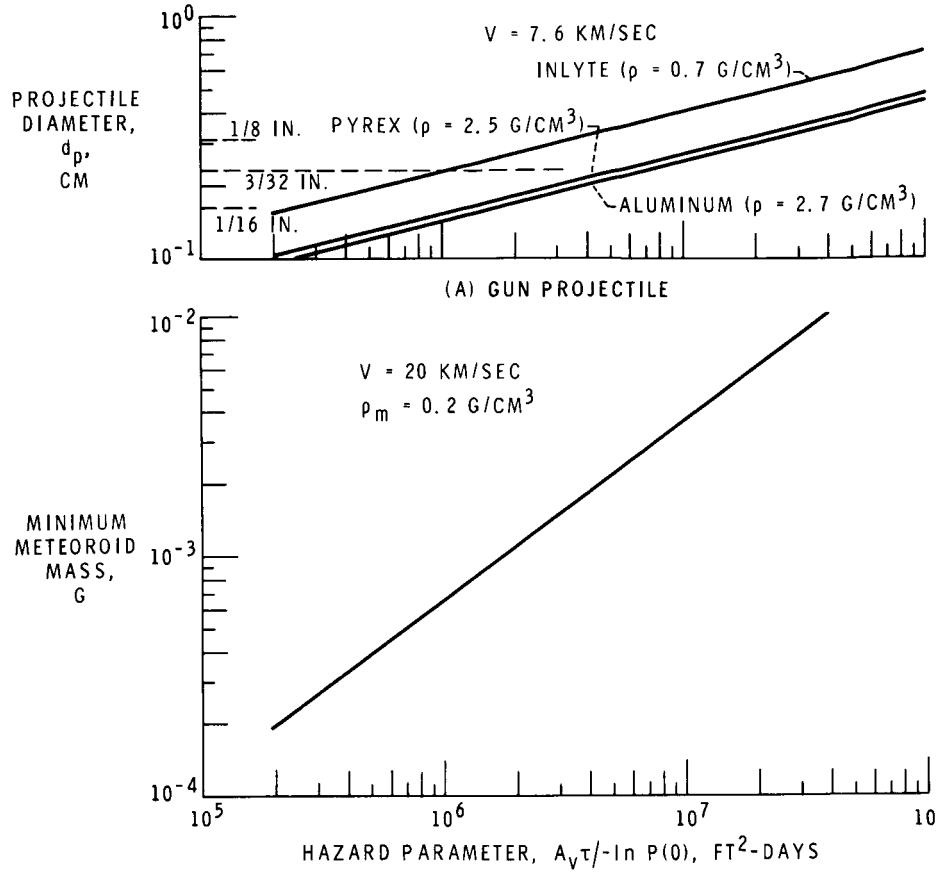

FIG. 3. - METEOROID AND PROJECTILE-PARTICLE VARIATIONS FOR EQUAL KINETIC ENERGY.

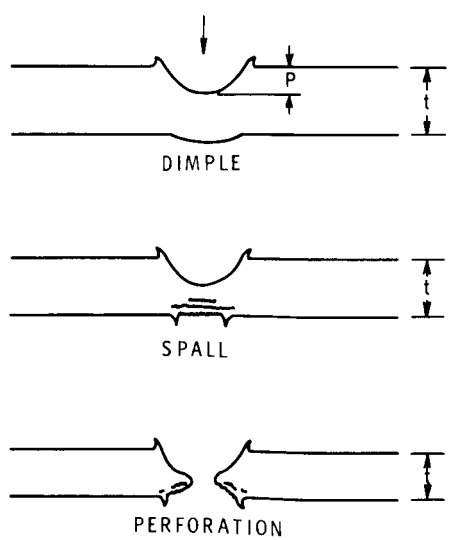

FIG. 4. - DEFINITION OF DAMAGE MODES.

MATERIAL	γ	a
316 STAINLESS STEEL	1.90	1.90
COLUMBIUM-1% ZIRCONIUM	1.49	2.10
PYROLYTIC GRAPHITE	2.41	1.75
EXPANDED PYROLYTIC GRAPHITE	2.77	1.60-1.75
ATJ GRAPHITE	1.14	1.75
BERYLLIUM	2.28	1.75

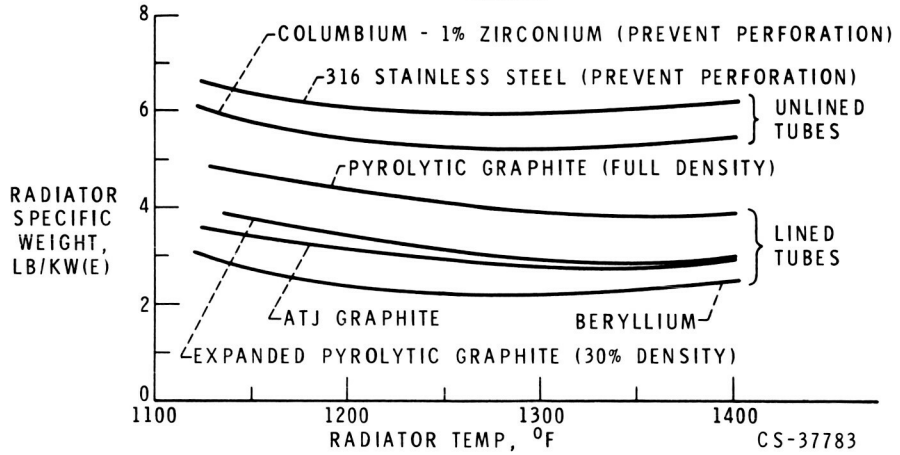

FIG. 5. - RADIATOR SPECIFIC WEIGHTS, 300 KW(E), 10,000 HOURS, P(0) = 0.96.

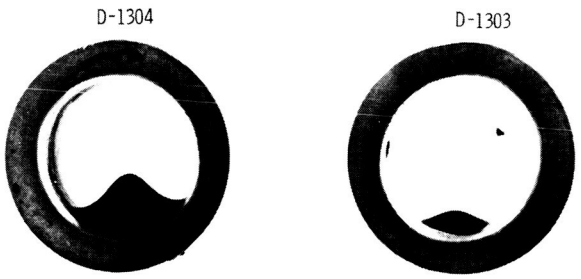

FIG. 6. - ALUMINUM ARMOR ON 316 STAINLESS STEEL LINER; PROJECTILE DIAMETER, 3/32 IN.; VELOCITY, 25,000 FPS.

(C-65983) (C-73675) (C-73099)

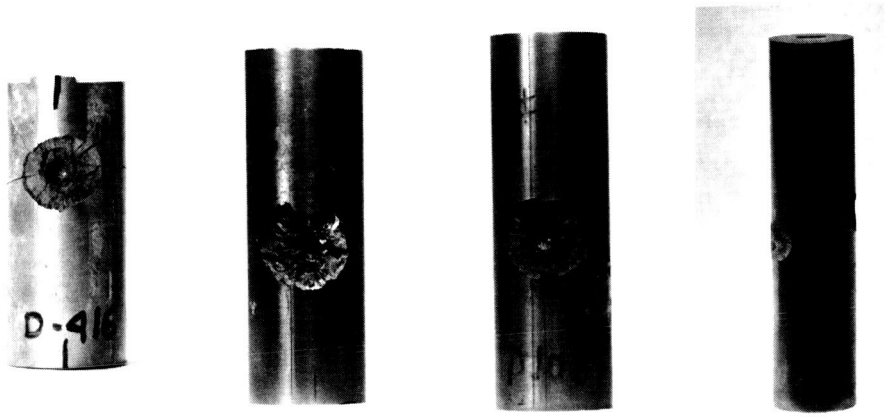

SINTERED POWDER | FIBER REINFORCED SINTERED POWDER | MESH REINFORCED SINTERED POWDER | SINTERED POWDER MULTIPLE IMPACT

CS-36499

FIG. 7. - BERYLLIUM-ARMORED TUBES AFTER TESTING AT 1300° F.

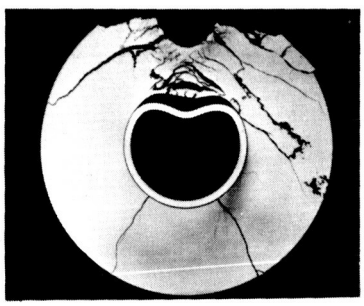

NO INTERNAL REINFORCEMENT

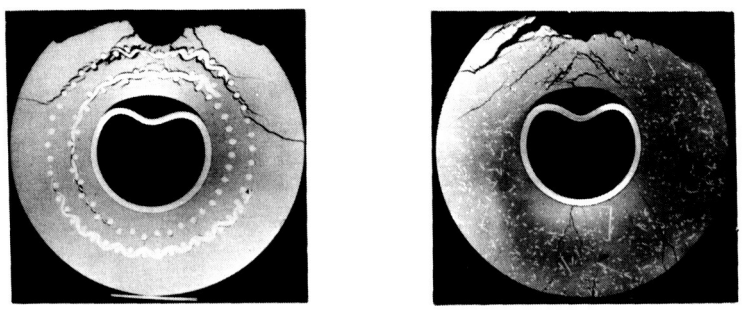

AISI 316 S.S. MESH REINFORCEMENT | AISI 316 S.S. FIBER REINFORCEMENT

CS-37575

FIG. 8. - BERYLLIUM-ARMORED TUBES AFTER IMPACT; TEST TEMPERATURE, 1300° F.

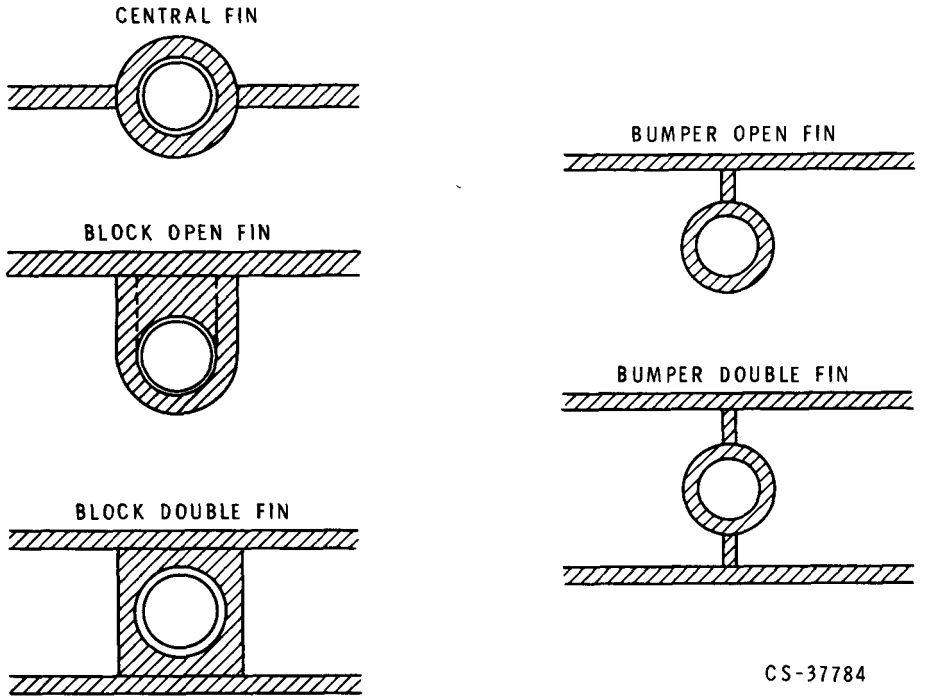

FIG. 9. - CONDUCTING FIN TUBE GEOMETRIES.

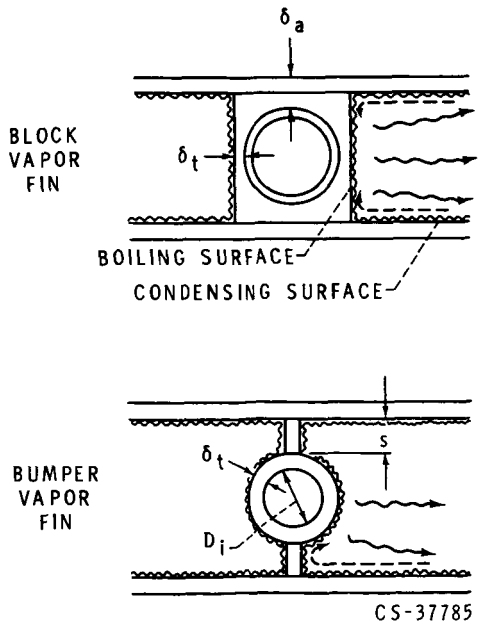

FIG. 10. - VAPOR FIN TUBE GEOMETRIES.

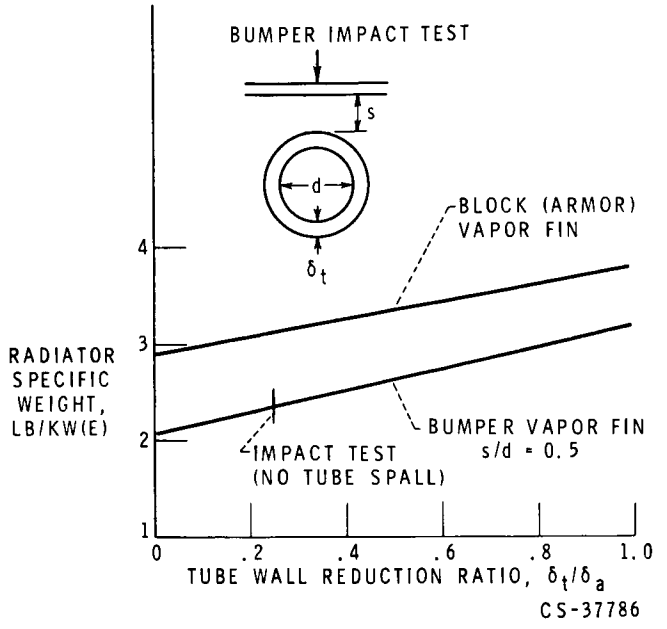

FIG. 11. - STAINLESS STEEL VAPOR FINS. 500 KW(E), 10,000 HRS, P(O) = 0.92.

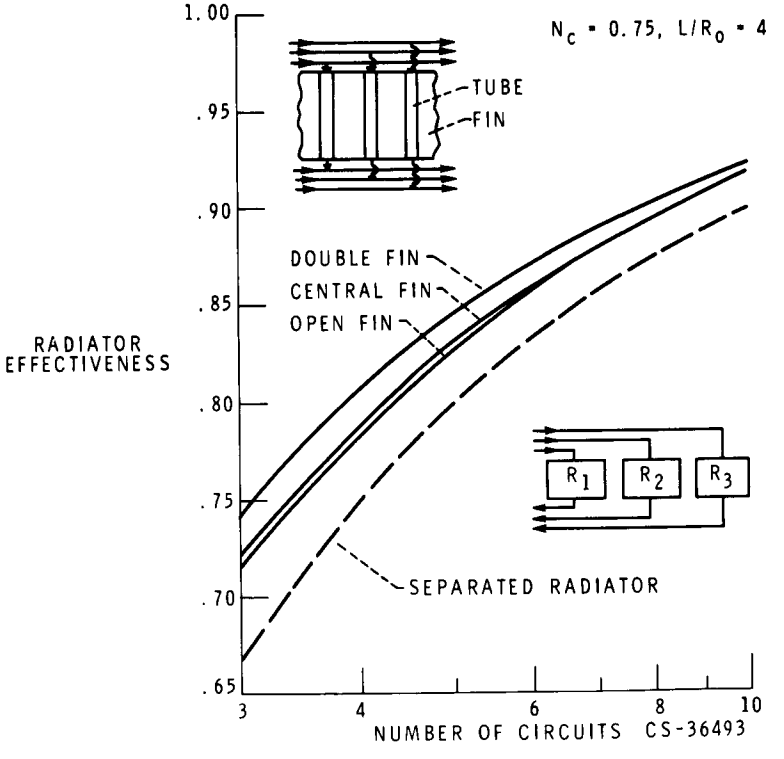

FIG. 12. - SHARED FIN RADIATOR EFFECTIVENESS.

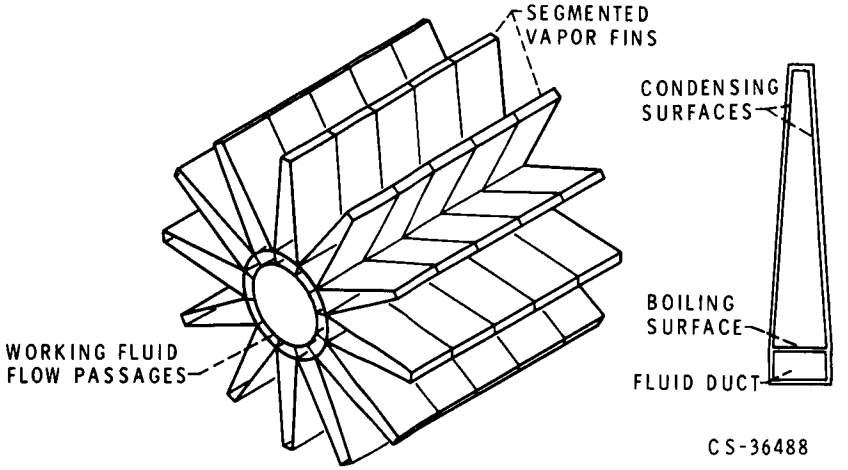

FIG. 13. - VAPOR FIN CONDENSER.